IEEE Photonics Journal
An IEEE Photonics Society Publication

Open Access

Reliable Integrated Photonic Light Sources Using Curved $Al_2O_3:Er^{3+}$ Distributed Feedback Lasers

Volume 9, Number 4, August 2017

Purnawirman
Nanxi Li
Gurpreet Singh
Emir Salih Magden
Zhan Su
Neetesh Singh
Michele Moresco
Gerald Leake
Jonathan D. B. Bradley
Michael R. Watts

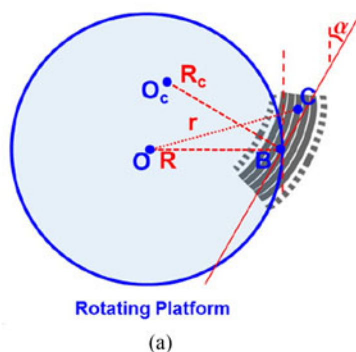

(a)

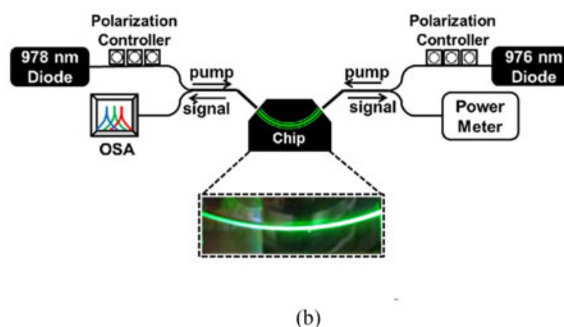

(b)

DOI: 10.1109/JPHOT.2017.2723947
1943-0655 © 2017 IEEE

IEEE photonics SOCIETY
IEEE

Reliable Integrated Photonic Light Sources Using Curved $Al_2O_3:Er^{3+}$ Distributed Feedback Lasers

Purnawirman,[1] Nanxi Li,[1,2] Gurpreet Singh,[1] Emir Salih Magden,[1] Zhan Su,[1] Neetesh Singh,[1] Michele Moresco,[1] Gerald Leake,[3] Jonathan D. B. Bradley,[1,4] and Michael R. Watts[1]

[1]Research Laboratory of Electronics, Massachusetts Institute of Technology, Cambridge, MA 02139 USA
[2]John A. Paulson School of Engineering and Applied Science, Harvard University, Cambridge, MA 02138 USA
[3]College of Nanoscale Science and Engineering, University at Albany, Albany, NY 12203 USA
[4]Current address: Department of Engineering Physics, McMaster University, Hamilton, ON L8S 4L7, Canada

DOI:10.1109/JPHOT.2017.2723947
1943-0655 © 2017 IEEE. Translations and content mining are permitted for academic research only. Personal use is also permitted, but republication/redistribution requires IEEE permission. See http://www.ieee.org/publications_standards/publications/rights/index.html for more information.

Manuscript received May 9, 2017; revised June 27, 2017; accepted July 2, 2017. Date of publication July 7, 2017; date of current version July 28, 2017. This work was supported in part by the Defense Advanced Research Projects Agency E-PHI under Grant HR0011-12-2-0007 project. N. Li is sponsored by the National Science Scholarship from the Agency of Science, Technology and Research (A*STAR), Singapore. Corresponding author: N. Li (e-mail: nanxili@mit.edu).

Abstract: We propose a curved erbium doped aluminum oxide ($Al_2O_3:Er^{3+}$) distributed feedback (DFB) laser for a reliable integrated photonics light source. The curved structure allows us for compensation of the radially varying film thickness due to the $Al_2O_3:Er^{3+}$ deposition process. In a conventional straight DFB structure, we observe randomly distorted transmission responses and relatively higher threshold power even for an estimated $<0.5\%$ thickness variation. The transmission response of the curved DFB laser shows good agreement with an ideal DFB structure of uniform thickness. We show 1.2 mW output power with a threshold power of 16 mW, demonstrating >6 times lower threshold compared to the straight DFB laser.

Index Terms: Integrated optics, integrated optics devices, lasers, guided waves.

1. Introduction

High quality, single frequency on-chip light sources are required for many applications in silicon photonics technology [1]–[5]. Erbium doped aluminum oxide ($Al_2O_3:Er^{3+}$) distributed feedback (DFB) lasers [6]–[10] offer a competitive alternative to hybrid III-V silicon lasers [11]–[16] for high power [6], narrow linewidth [9], [10], and thermally stable [17]–[19] integrated light sources. A CMOS-compatible waveguide design generally consists of a silicon nitride (SiN_x) guiding layer followed by a backend-deposited active film [7], [20]–[23]. Thin $Al_2O_3:Er^{3+}$ films have been consistently grown by many research groups using a reactive co-sputtering process first described by Wörhoff *et al.* [24]. In a standard sputtering system, the substrate is mounted on a rotating platform with a radially

varying film thickness profile from the center. Thus, a conventional straight DFB structure would experience small thickness non-uniformity along the cavity.

We investigate the influence of film thickness uniformity on cavity Q and threshold power in Al_2O_3:Er^{3+} DFB lasers, and experimentally measure the thickness variation of the film across a 5-cm radius platform. We show that in a 2-cm-long Al_2O_3:Er^{3+} DFB laser even for thickness variations of $<$0.5%, the cavity response can be highly distorted with significantly reduced Q. A shorter cavity would reduce the thickness variation across the DFB laser, while it limits the single pass absorption efficiency of the pump power. To improve the absorption rate, a higher doping concentration may be considered at the expense of increase in energy-transfer upconversion (ETU) [25] and ion quenching [26]–[28]. Alternatively, the thickness variation can be compensated by introducing a refractive-index varying waveguide along the cavity. This approach would require a more complex design that includes varying film thickness, waveguide dimensions, and DFB cavity parameters to provide the right compensating values in the device.

In this paper, we propose a compensation scheme based on a curved DFB structure that follows the circular symmetry of the deposition system. Under the same grating parameters, an output power of 1.2 mW is achieved in a curved DFB laser, demonstrating $>$6 times lower threshold power compared to a straight DFB laser. The transmission response of the curved DFB structure shows agreement with the ideal DFB structure of uniform thickness.

We organize our discussions in this report by the following. In Section 2, we analyze the influence of thickness variation on the performance of a straight DFB laser. We discuss the compensation scheme using a curved DFB structure in Section 3. Then in Section 4, we experimentally compare the performance of curved vs. straight DFB lasers. Section 5 provides further discussion of the approach. Finally, we present our summary in Section 6.

2. Analysis of Thickness Variation in Straight DFB Laser

We measure the thickness variation of an Al_2O_3:Er^{3+} film deposited in a reactive sputtering system (AJA ATC Orion) which used 2” Er and Al sputtering targets in a confocal arrangement. The substrate is mounted on a 5-cm-radius rotating platform. After deposition, thickness measurements are performed by prism coupling at various distances R from the center of the platform. Several film depositions in the range of 1000–1500 nm are normalized as shown in Fig. 1(a). The data is fitted with a quadratic polynomial function, estimating 12% maximum variation across the platform.

Fig. 1(b) illustrates a top view of the rotating platform with a straight DFB structure. Different parts of the DFB structure are located at varying distances r from the center O, thus inducing thickness variation along the device. Furthermore, a non-zero tilt angle α within rotational plane, as shown in top view, can introduce additional skew to the profile. This misalignment can also be interpreted as translational error of (x_{shift}, y_{shift}) from position where $\alpha = 0$ (point A). These parameters can be calculated with equation (1)–(3).

$$r_{(d)}^2 = (R + d \sin\alpha)^2 + (d \cos\alpha)^2 \quad (1)$$

$$x_{shift} = R(1 - \cos\alpha) \quad (2)$$

$$y_{shift} = R \sin\alpha, \quad (3)$$

where for a DFB with length of D_{DFB}, d is calculated from $-D_{DFB}/2$ to $+D_{DFB}/2$.

The thickness variation along the DFB cavity is illustrated in Fig. 1(c). The cavity with length D_{DFB} and grating period Λ is deposited with base Al_2O_3:Er^{3+} thickness of T_0. The variation Δt along the cavity is skewed for $\alpha \neq 0$. We calculate the thickness variation for various tilt angles, $D_{DFB} = 2$ cm, and positioning at $R = 3$ cm, as shown in Fig. 1(d). The thickness is normalized for $T_0 \approx 1100$ nm. We obtain a small non-uniformity of 0.5%, 0.6%, and 0.8% for $\alpha = 0^\circ$, 2.5°, and 5° respectively.

The influence of film thickness non-uniformity on cavity Q is investigated for different magnitude of the variations, as shown in Fig. 2. Using a transfer matrix calculation (in-house Matlab code), we calculate the transmission response of straight DFB cavities for various tilt angles (row-wise) and thickness variations (column-wise). The DFB is segmented into 1000 sections, with the effective

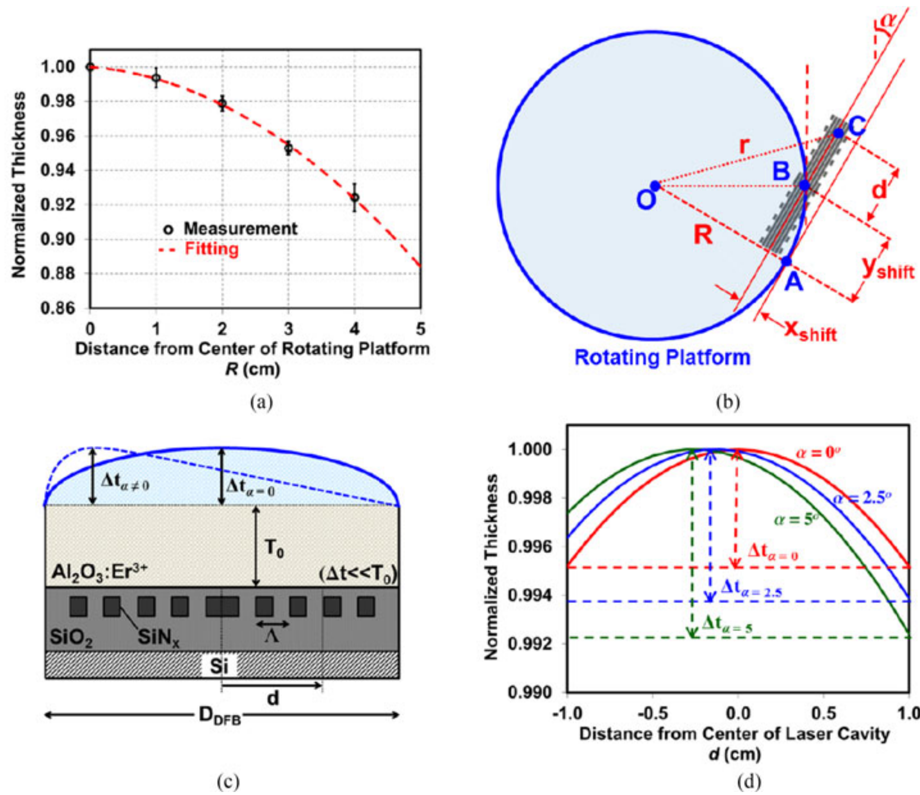

Fig. 1. (a) Measurement (black) of the Al_2O_3 film thickness fitted with a quadratic function (red) at varying distance from the center of the rotating deposition platform. (b) Diagram of the straight DFB laser placement in a radially symmetric Al_2O_3 film deposition process. (c) Illustration of thickness variation along the Al_2O_3:Er^{3+} DFB cavity. (d) Calculation of thickness profile in 2-cm-long straight DFB cavities for various tilt angles at R = 3 cm.

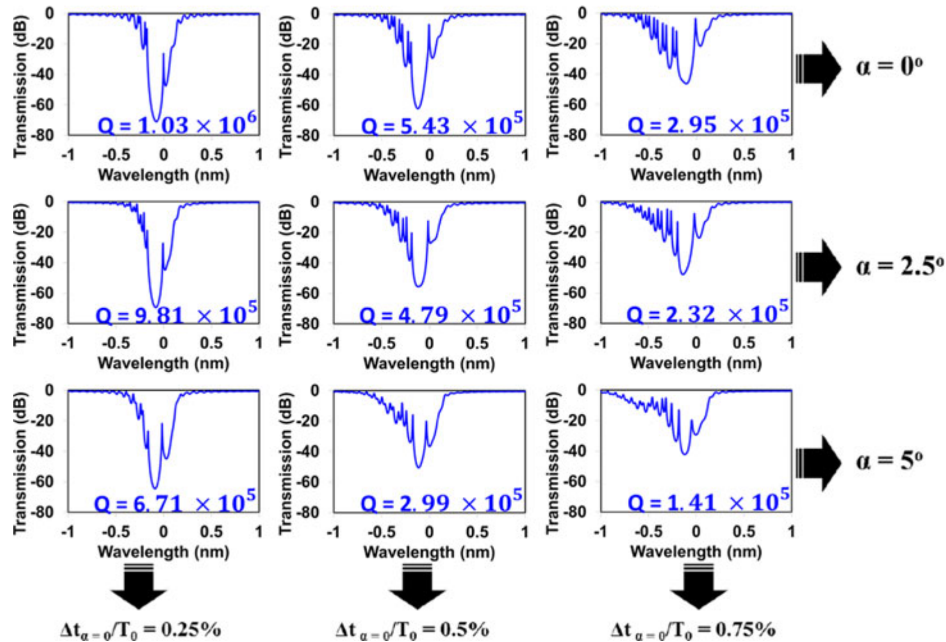

Fig. 2. Calculation of transmission response of straight 2 cm DFB cavity for various tilt angles and thickness variations at $R = 3$ cm using transfer matrix method.

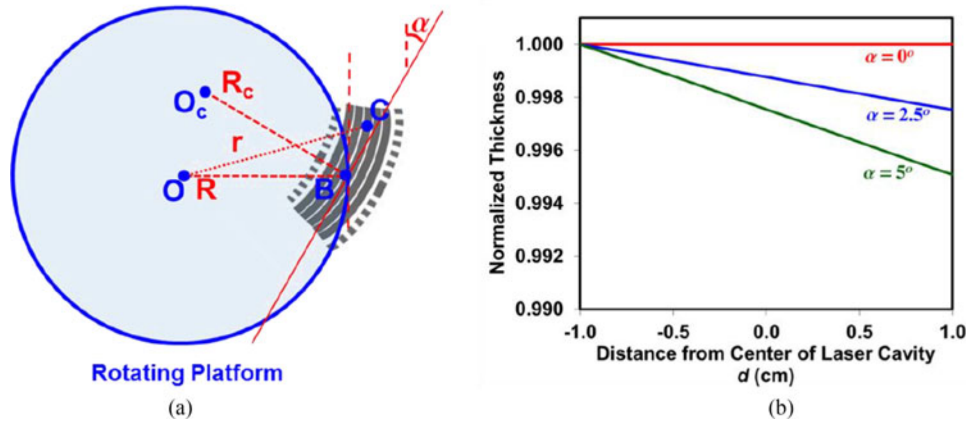

Fig. 3. (a) Diagram of the curved DFB laser placement in a radially symmetric Al_2O_3:Er^{3+} film deposition chamber. (b) Calculation of thickness profile in a 2 cm long curved DFB cavity for various tilt angles at $R = R_c = 3\,\text{cm}$.

index n_{eff} as a function of the film thickness at different d. The grating has strength $\kappa = 0.5\,\text{mm}^{-1}$, length $D_{DFB} = 2\,\text{cm}$, and total absorption loss $l = 0.5\,\text{dB}$. The Q factor is determined from the ratio of the laser resonant wavelength $\lambda = 1590\,\text{nm}$ with the 3-dB width of the resonance peak. We observe distortions and asymmetries in the transmission response that reduce the cavity Q significantly compared to uniform thickness DFB ($Q_{max} = 1.07 \times 10^6$) with symmetric transmission response.

3. Compensation Scheme by Curved DFB Structure

To compensate for the thickness non-uniformity in the deposition, we propose a curved DFB structure that follows the circular symmetry of the platform, as shown in Fig. 3(a), where R is the distance between the center of deposition platform to the geometry center of the DFB, and R_c is the distance between the DFB curvature center to its geometry center. By placing the curved DFB at $R = R_c$ (the DFB curvature center O_c and the center of the platform O coincide), a uniform thickness profile can be maintained throughout the cavity. The calculated thickness profile of a 2 cm-long curved DFB structure at various angles shows that the profile is linear with smaller magnitude of variation, as shown in Fig. 3(b). The radial distance r as a function of position in the device d is calculated by the following formula:

$$r_{(d)}^2 = (x_{shift} + x'_{(d)}\cos\alpha + y'_{(d)}\sin\alpha)^2 + (y_{shift} - x'_{(d)}\sin\alpha + y'_{(d)}\cos\alpha)^2, \tag{4}$$

where (x_{shift}, y_{shift}) denotes the relative position of the DFB curvature center (point O_c) to the center of the platform (point O), and $(x'_{(d)}, y'_{(d)})$ is the position of a segment in the device (point C) relative to point O_c. These parameters can be calculated by the following relations:

$$x_{shift} = R - R_c\cos\alpha \tag{5}$$

$$y_{shift} = R_c\sin\alpha \tag{6}$$

$$x'_{(d)} = R_c\cos(d/R_c) \tag{7}$$

$$y'_{(d)} = R_c\sin(d/R_c). \tag{8}$$

Fig. 4 shows the transmission responses of curved DFB cavities under the same parameters shown in Fig. 3. Compared with the distorted asymmetric transmission response in Fig. 2, the curved DFBs maintain symmetric transmission responses and outperform the Q factors of the straight DFB structures. The cavity Q only suffers noticeable degradation after a misalignment of

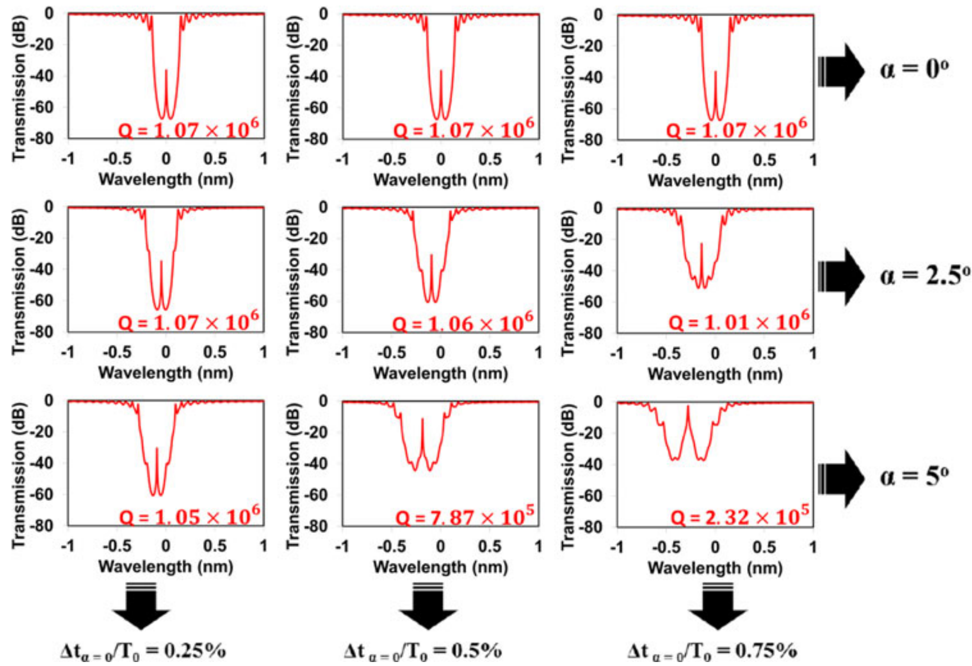

Fig. 4. Calculation of transmission response of curved 2 cm DFB cavity for various tilt angles and thickness variations at $R = 3$ cm using transfer matrix method.

$\alpha \approx 5^\circ$ for $\Delta t_{\alpha=0}/T_0 > 0.5\%$. This illustrates the enhanced fabrication tolerance of the curved DFB design.

4. Experimental Measurement of Curved Versus Straight DFB Laser

The laser structures were first fabricated in a state-of-the-art complementary metal-oxide semiconductor (CMOS) foundry on a 300 mm silicon wafer. The Si_3N_4 layer was deposited on top of a 6 μm-thick SiO_2 layer, and patterned using 193-nm immersion lithography. Next, a SiO_2 layer was deposited on top of the wafer followed by a planarization process. The wafer is then diced into individual chips for active material deposition as a post-processing step. The deposition process with more detail has been reported in [29], with the only difference in layer thickness and dopant. We compare the performance of straight and curved Al_2O_3:Er^{3+} DFB lasers fabricated on the same chip. Each laser chip was placed individually into the deposition chamber and aligned manually at R $\approx$ 3 cm in the platform. Though, at present, the placement, alignment of the chips and deposition steps are performed manually as a demonstration, in the future, the whole post-processing of the curved laser chips to the right curvature in the chamber can be automated, making it a practical solution for a chip-level production line. We use a multi-segmented wavelength-insensitive design [30] that consists of a silicon (Si) substrate, five SiN_x segments (thickness of 200 nm, width of 450 nm, and gap of 400 nm), enclosed by a SiO_2 layer (oxide gap of 200 nm), and Al_2O_3:Er^{3+} gain film (thickness $T_0 = 1100$ nm). A discrete quarter phase shift is formed at the center of each cavity to produce sharp resonances at the Bragg condition. The grating is formed by additional periodic pieces on both sides with fixed period $\Lambda = 502$ nm ($\lambda_{laser} \approx$ 1590 nm) for both curved and straight DFB cavities. These periodic side pieces have width of 300 nm and gap distance of 350 nm. For curved DFB design, there is no grating period change between the outside and the inside curve since the grating period (in nm scale) is much less than the radius of curvature (in cm scale). We use the prism coupling method to estimate a background loss of <0.1 dB/cm and dopant concentration of 1.0×10^{20} cm^{-3} by linear fitting of measured total film loss vs. the film absorption cross-section around 1550 nm [30].

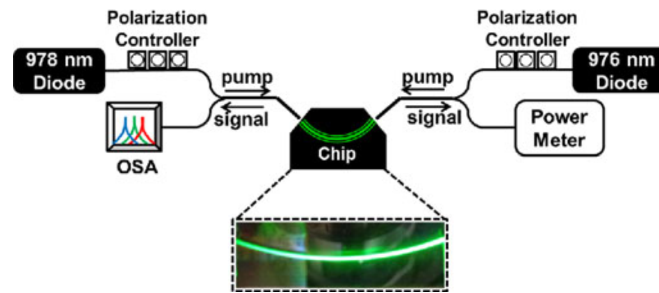

Fig. 5. Experimental setup used for curved $Al_2O_3:Er^{3+}$ DFB laser.

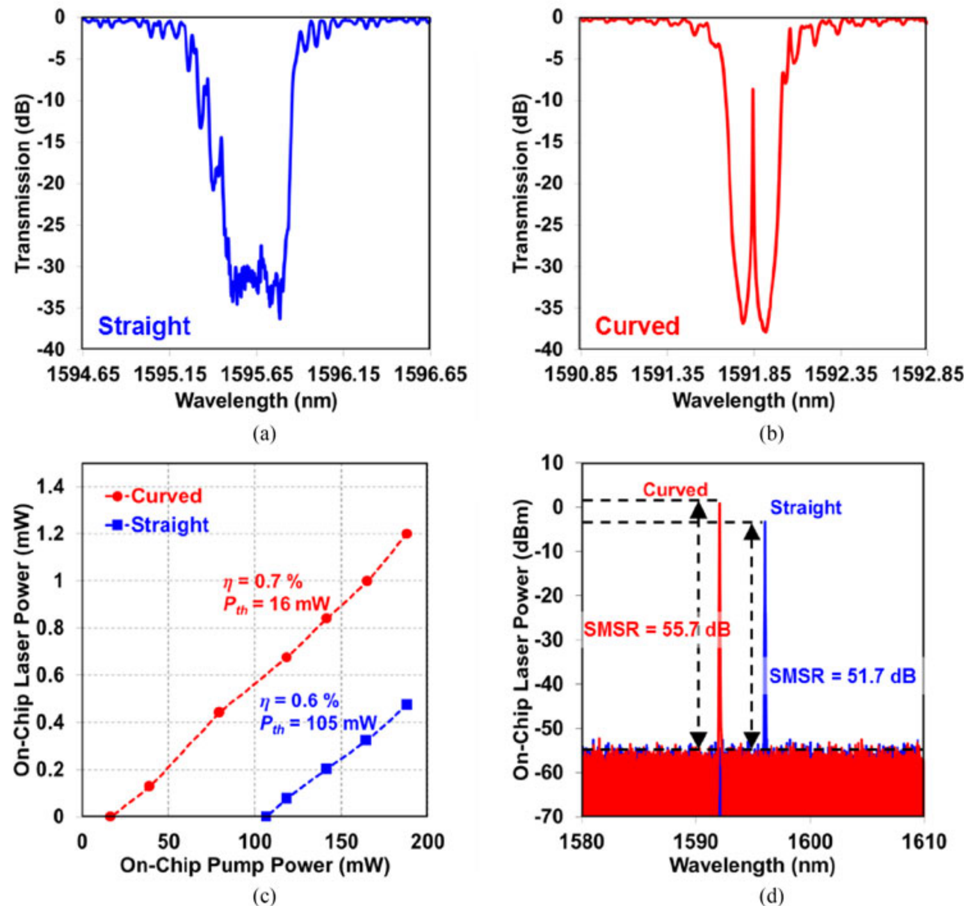

Fig. 6. Experimental measurement of straight and curved $Al_2O_3:Er^{3+}$ DFB lasers. (a) Transmission measurement of straight DFB cavity. (b) Transmission measurement of curved DFB cavity. (c) Comparison of output powers of straight and curved DFB lasers at different pump powers. (d) Optical spectra of straight and curved DFB lasers.

Fig. 5 shows the experimental setup used for lasing signal measurement. For the curved DFB structure, the chip edge is angle-etched to provide normally-incident coupling from a fiber. A tunable laser system (Agilent 81600B) is used for transmission measurement of unpumped lasers. Fig. 6(a) and (b) show the measurement results of the unpumped straight and curved DFB lasers, respectively. The straight DFB structure contains similar features to those calculated in Fig. 2, with many distorted peaks emerging in the blue-shifted wavelengths of the resonance. The resonance peak does not have a clear 3-dB bandwidth for Q estimation. The curved DFB structure shows

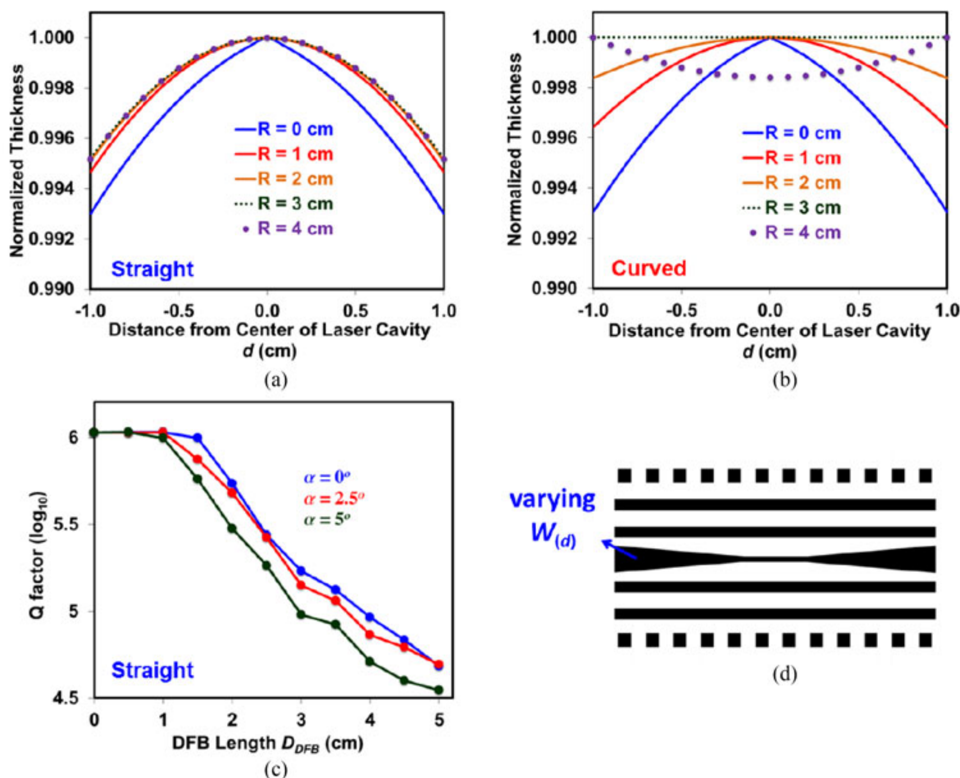

Fig. 7. (a) Calculation of Al_2O_3:Er^{3+} film thickness profile for straight DFB lasers with $\alpha = 0^\circ$ at various radial distances R from the center of the deposition platform. (b) Calculation of Al_2O_3:Er^{3+} thickness profile for curved DFB lasers with $R_c = 3$ cm and $\alpha = 0^\circ$ at various radial distances R from the platform center. (c) Plot of Q factor of straight DFB lasers for various DFB lengths at $R = 3$ cm. (d) Illustration of an effective-index-varying waveguide design.

a symmetric response, with measured $Q = 4.55 \times 10^5$. The discrepancy between transmittance measurement (Fig. 5(a) and (b)) and simulation (Figs. 2 and 4) are due to the limitation in estimating the system's parameters, as summarized in following: (I) Uncertainty in loss estimation: we use a lower bound estimate of the laser loss for the simulation. While this may not be ideal for real device. The real device loss is contributed by waveguide sidewall roughness and propagation loss in material (Si_3N_4, Al_2O_3, SiO_2), and it's likely to be higher than our current estimated number. (II) Uncertainty in thickness profile: the thickness profile in the simulation is estimated by interpolating the thickness measurements at several points from the film's center. We agree a better thickness profile measurements would help in obtaining better-fitted simulation result. (III) Uncertainty in gain estimation: due to varying condition in the Al_2O_3:Er^{3+} film deposition, the simulation of the laser dynamics should depend on the gain characteristic of the material. We include the work by Agazzi (2012) [31] for the thorough examination of Al_2O_3:Er^{3+} gain parameters.

We pump the DFB lasers from both sides using fiber pigtail laser diodes at 978 nm and 976 nm. Fig. 6(c) shows >6 times improvement in the threshold power for the curved DFB ($P_{th} = 16$ mW) compared to the straight DFB ($P_{th} = 105$ mW) laser, with similar slope efficiencies (0.6–0.7%). At a total pump power of 188 mW, we obtain a maximum output power of 1.2 mW for the curved DFB laser and less than 0.5 mW for the straight DFB laser. Lastly, Fig. 6(d) shows the output spectra of both lasers, demonstrating a side mode suppression ratio (SMSR) of 55.7 dB for the curved DFB laser. Additionally, though straight laser has been demonstrated before with lasing threshold of 14 mW and slope efficiency of 2.9% in [30], the design parameters (eg. Phase shifted region length) are different from the one used here, therefore not an exact comparison that should be used to compare with the current curved laser.

5. Further Discussion

In Fig. 7(a) and (b), we consider the sensitivity of 2 cm straight and curved DFB thickness profiles to the position in platform. For the straight DFB structure, the thickness variation is similar for all R, with a magnitude of around 0.5%. For the curved DFB structure ($R_c = 3\,cm$), a thickness variation $<$0.2% can be obtained by placing the substrate between $2\,cm < R < 4\,cm$. Our laser design can also be curved at different curvatures. Correspondingly, the placement of the substrate will be changed to match the laser curvature. This reinforces the fabrication tolerance and the reliability of the curved DFB structure.

We also consider the effect of the device length. Q factors of straight DFBs with various lengths are shown in Fig. 7(c), for $\alpha = 0^\circ$, 2.5° and 5°. Shorter ($<1\,cm$) structures accumulate smaller thickness non-uniformity, thus providing a more reliable design for straight DFB cavities. However, to achieve a similar power efficiency, such shorter DFBs might require a higher doping concentration which can be detrimental to the laser performance [32].

An alternative approach is to design an effective index varying waveguide along the cavity. The SiN_x waveguide width can be adjusted along the cavity to provide the required compensation value for the thickness variations, as illustrated in Fig. 7(d). The compensating values have to be customized for each selection of waveguide dimensions (thickness and width of each layer) and it also requires good prior calibration of the entire process. Last but not least, the thickness non-uniformity can be improved by using larger sputtering targets in the tool, or by using more advanced tools (eg. HELIOS series of Leybold Optics using plasma-assisted reactive magnetron sputtering with optical monitoring, should be able to provide better uniformity [33]). Meanwhile, those tools are generally costly, making them not cost-effective for general sputtering purpose.

6. Conclusion

We investigate the influence of $Al_2O_3:Er^{3+}$ film thickness uniformity on cavity Q and threshold power in $Al_2O_3:Er^{3+}$ DFB lasers. For thickness variations of $<$0.5% in a 2-cm-long straight DFB cavity, the transmission response can be highly distorted with significantly reduced Q. We propose a compensation scheme based on a curved DFB structure that follows the circular symmetry of the $Al_2O_3:Er^{3+}$ thin film deposition system. Under the same deposition conditions and grating parameters, the curved design outperformed the conventional straight DFB structure. We achieve a slope efficiency of 0.7%, threshold power of 16 mW, and maximum output power of 1.2 mW for the curved DFB laser. In the straight DFB laser, we obtain a slope efficiency of 0.6%, threshold power of 105 mW, and maximum output power of 0.5 mW, demonstrating $>$6 times threshold power improvement.

Acknowledgment

The authors would like to thank Dr. E. Bernhardi and Dr. J. Conway for the helpful discussions.

References

[1] A. Alduino *et al.*, "Demonstration of a high speed 4-channel integrated silicon photonics WDM link with hybrid silicon lasers," in *Proc. Int. Conf. Integr. Photon. Res. Silicon Nanophoton. Photon. Switching*, Monterey, CA, USA, 2010, Paper PDIWI5.

[2] C. H. Chen *et al.*, "DWDM silicon photonic transceivers for optical interconnect," in *Proc. 2015 Int. Conf. IEEE Opt. Interconnects*, 2015, pp. 52–53.

[3] S. Tanaka *et al.*, "Four-wavelength silicon hybrid laser array with ring-resonator based mirror for efficient CWDM transmitter," in *Proc. 2013 Int. Conf. Expo. Opt. Fiber Commun. Nat. Fiber Opt. Eng.*, 2013, pp. 1–3.

[4] M. J. R. Heck *et al.*, "Hybrid Silicon photonic integrated circuit technology," *IEEE J. Sel. Topics Quantum. Electron.*, vol. 19, no. 4, Jul./Aug. 2013, Art. no. 6100117.

[5] L. Tao *et al.*, "4-λ InGaAsP-Si distributed feedback evanescent lasers with varying silicon waveguide width," *Opt. Exp.*, vol. 22, pp. 5448–5454, 2014.

[6] E. S. Hosseini *et al.*, "CMOS-compatible 75 mW erbium-doped distributed feedback laser," *Opt. Lett.*, vol. 39, pp. 3106–3109, 2014.

[7] M. Belt and D. J. Blumenthal, "Erbium-doped waveguide DBR and DFB laser arrays integrated within an ultra-low-loss Si3N4 platform," *Opt. Exp.*, vol. 22, pp. 10655–10660, 2014.
[8] G. Singh *et al.*, "Resonant pumped erbium-doped waveguide lasers using distributed Bragg reflector cavities," *Opt. Lett.*, vol. 41, pp. 1189–1192, 2016.
[9] E. H. Bernhardi *et al.*, "Ultra-narrow-linewidth, single-frequency distributed feedback waveguide laser in Al_2O_3:Er^{3+} on silicon," *Opt. Lett.*, vol. 35, pp. 2394–2396, 2010.
[10] M. Belt, T. Huffman, M. L. Davenport, W. Li, J. S. Barton, and D. J. Blumenthal, "Arrayed narrow linewidth erbium-doped waveguide-distributed feedback lasers on an ultra-low-loss silicon-nitride platform," *Opt. Lett.*, vol. 38, pp. 4825–4828, 2013.
[11] O. Bondarenko, Q. Gu, J. Shane, A. Simic, B. Slutsky, and Y. Fainman, "Wafer bonded distributed feedback laser with sidewall modulated Bragg gratings," *Appl. Phys. Lett.*, vol. 103, 2013, Art. no. 043105.
[12] L. Grenouillet *et al.*, "Hybrid integration for silicon photonics applications," *Opt. Quantum Electron.*, vol. 44, pp. 527–534, 2012.
[13] B. R. Koch *et al.*, "Mode locked and distributed feedback silicon evanescent lasers," *Laser Photon. Rev.*, vol. 3, pp. 355–369, 2009.
[14] S. Stankovic, R. Jones, M. N. Sysak, J. M. Heck, G. Roelkens, and D. Van Thourhout, "Hybrid III-V/Si distributed-deedback laser based on adhesive bonding," *IEEE Photon. Technol. Lett.*, vol. 24, no. 23, pp. 2155–2158, Dec. 2012.
[15] A. W. Fang, P. Hyundai, R. Jones, O. Cohen, M. J. Paniccia, and J. E. Bowers, "A continuous-wave hybrid AlGaInAs-silicon evanescent laser," *IEEE Photon. Technol. Lett.*, vol. 18, no. 10, pp. 1143–1145, May 2006.
[16] S. S. Sui, M. Y. Tang, Y. D. Yang, J. L. Xiao, Y. Du, and Y. Z. Huang, "Sixteen-wavelength hybrid AlGaInAs/Si microdisk laser array," *IEEE J. Quantum. Electron.*, vol. 51, no. 4, Apr. 2015, Art. no. 2600108.
[17] Purnawirman *et al.*, "Wavelength division multiplexed light source monolithically integrated on a silicon photonics platform," *Opt. Lett.*, vol. 42, pp. 1772–1775, 2017.
[18] N. Li *et al.*, "Athermal synchronization of laser source with WDM filter in a silicon photonics platform," *Appl. Phys. Lett.*, vol. 110, no. 21, 2017, Art. no. 211105.
[19] M. Belt and D. J. Blumenthal, "High temperature operation of an integrated erbium-doped DBR laser on an ultra-low-loss Si3N4 platform," in *Proc. Int. Conf. Exhib. Opt. Fiber Commun.*, 2015, pp. 1–3.
[20] Z. Su *et al.*, "Ultra-compact CMOS-compatible ytterbium microlaser," in *Proc. Int. Conf. Integr. Photon. Res. Silicon Nanophoton.*, 2016, Paper IW1A.3.
[21] N. Li *et al.*, "High-power thulium lasers on a silicon photonics platform," *Opt. Lett.*, vol. 42, pp. 1181–1184, 2017.
[22] Z. Su *et al.*, "Ultra-compact and low-threshold thulium microcavity laser monolithically integrated on silicon," *Opt. Lett.*, vol. 41, pp. 5708–5711, 2016.
[23] C. M. Sorace-Agaskar *et al.*, "Integrated mode-locked lasers in a CMOS-compatible silicon photonic platform," in *Proc. Int. Conf. Laser Electro-Opt.*, 2015, Paper SM2I.5.
[24] K. Wörhoff, J. D. B. Bradley, F. Ay, D. Geskus, T. P. Blauwendraat, and M. Pollnau, "Reliable low-cost fabrication of low-loss Al_2O_3:Er^{3+} waveguides with 5.4-dB optical gain," *IEEE J. Quantum Electron.*, vol. 45, no. 5, pp. 454–461, Jun. 2009.
[25] L. Agazzi, K. Wörhoff, and M. Pollnau, "Energy-transfer-upconversion models, their applicability and breakdown in the presence of spectroscopically distinct ion classes: A case study in amorphous Al_2O_3:Er^{3+}," *J. Phys. Chem. C*, vol. 117, pp. 6759–6776, 2013.
[26] F. Sanchez, P. Le Boudec, P.-L. François, and G. Stephan, "Effects of ion pairs on the dynamics of erbium-doped fiber lasers," *Phys. Rev. A*, vol. 48, pp. 2220–2229, 1993.
[27] N. Li, J. D. B. Bradley, G. Singh, E. S. Magden, J. Sun, and M. R. Watts, "Self-pulsing in Erbium-doped fiber laser," in *Proc. Int. Conf. Optoelectron. Global*, 2015, pp. 1–2.
[28] S. Colin, E. Contesse, P. Le Boudec, G. Stephan, and F. Sanchez, "Evidence of a saturable-absorption effect in heavily erbium-doped fibers," *Opt. Lett.*, vol. 21, pp. 1987–1989, 1996.
[29] J. D. B. Bradley *et al.*, "1.8-μm thulium microlasers integrated on silicon," *Proc. SPIE*, vol. 9744, 2016, Art. no. 97440U.
[30] Purnawirman *et al.*, "Ultra-narrow-linewidth Al_2O_3:Er^{3+} lasers with a wavelength-insensitive waveguide design on a wafer-scale silicon nitride platform," *Opt. Exp.*, vol. 25, pp. 13705–13713, 2017.
[31] L. Agazzi, "Spectroscopic excitation and quenching processes in rare-earth-ion-doped Al_2O_3 and their impact on amplifier and laser performance," M.S. Thesis, Univ. Twente, Enschede, the Netherlands, 2012.
[32] L. Agazzi, E. H. Bernhardi, K. Wörhoff, and M. Pollnau, "Impact of luminescence quenching on relaxation-oscillation frequency in solid-state lasers," *Appl. Phys. Lett.*, vol. 100, 2012, Art. no. 011109.
[33] M. Scherer, U. Schallenberg, H. Hagedorn, W. Lehnert, B. Romanov, and A. Zoeller, "High performance notch filter coatings produced with PIAD and magnetron sputtering," *Proc. SPIE*, vol. 7101, 2008.